This is a previous version of the article published in Electrochimica Acta. 2021, 368: 137590. https://doi.org/10.1016/j.electacta.2020.137590

ELECTROCHEMICAL PERFORMANCE OF N-DOPED SUPERPOROUS ACTIVATED CARBONS IN IONIC LIQUID-BASED ELECTROLYTES

María José Mostazo-López[1], Jakob Krummacher[2], Andrea Balducci[2], Emilia Morallón[3], Diego Cazorla-Amorós[1*]

[1]*Instituto Universitario de Materiales, Departamento de Química Inorgánica, Universidad de Alicante, Apartado 99, 03080-Alicante, Spain*
[2]*Institute for Technical Chemistry and Environmental Chemistry and Center for Energy and Environmental Chemistry (CEEC), Philosophenweg 7a, 07743 Jena, Germany*
[3]*Instituto Universitario de Materiales, Departamento de Química Física, Universidad de Alicante, Apartado 99, 03080-Alicante, Spain*

*Corresponding author: Diego Cazorla-Amorós (cazorla@ua.es)

Abstract

The electrochemical performance of nitrogen-doped and non-doped superporous activated carbons as electrodes for supercapacitors was assessed in organic and ionic liquid-based electrolytes. The nitrogen functionalization was carried out through post-modification treatments at mild conditions to produce N-doped activated carbons that preserve the microporosity of the pristine carbon material. The electrodes based on these materials provide large capacitance values (up to 150-180 F/g) in both 1M $Pyr_{14}TFSI$/PC and 1M $Pyr_{14}BF_4$/PC due to their tailored porous texture, given by their well-developed microporosity and low mesopore volume. The electrochemical double layer capacitors based on these materials displayed outstanding capacitance (37-40 F/g and 14 F/cm^3) and energy values (44-48 Wh/kg and 16-17 Wh/L). The nitrogen-doped activated carbons evidence high stability at positive and negative polarization potentials due the presence of specific N functionalities. The results prove that surface chemistry of carbon materials plays a key role on their degradation under high operation voltage conditions. The durability of the devices can be improved by doping carbon electrodes with selected nitrogen groups, such as nitrogen heterocycles and amine-like surface functionalities.

Keywords: supercapacitors, nitrogen functionalization, superporous activated carbons, ionic liquid, electrochemical stability

1. Introduction

Electrochemical double-layer capacitors (EDLC), or supercapacitors, are currently the most suitable energy storage devices for a wide range of high-power applications. These devices are based on the physical electrosorption of ions at the interface of an electrode and an electrolyte [1–3]. Consequently, EDLC can be charged and discharged in seconds, providing high specific power (10 kW/kg) and long-cycle life (> 500.000 cycles). Nevertheless, the energy density needs to be increased to introduce this technology into new applications, such as electric vehicles. This parameter depends on the capacitance and the cut-off voltage employed during the operation of the device, which are mostly governed by the two main components of supercapacitors: the electrolyte and the electrode material. The current commercially available supercapacitors are based on activated carbons, whose large surface area produces high capacitance values, and organic electrolytes, based on solutions of an ammonium salt in propylene carbonate (PC) or acetonitrile, which can operate at 2.5-2.8 V [1,4]. One of the main strategies for improving their performance is the use of innovative electrolytes, such as those based on ionic liquids (ILs) or new conducting salts (in organic solvents), since they can expand the operation voltage to values larger than 3V [5,6].

The development of new electrolytes based on ILs has attracted considerable attention due to their wide electrochemical stability window (>3V), high thermal stability, low volatility and non-flammability [5,7–10]. However, their high viscosity and low conductivity (in comparison with conventional organic electrolytes) hinders the capacitance and power provided by EDLC based in solvent-free ILs. Recently, the use of mixtures of ILs with organic solvents (PC or acetonitrile), in which IL acts as a conducting salt, has appeared as a promising alternative because it allows the production of electrolytes with low viscosity and high conductivity. However, the operative voltage of EDLCs containing these electrolytes is often limited in comparison with that of EDLC based on solvent-free ILs, but still overcomes the values of conventional organic electrolytes.

An alternative to the use of ILs is the investigation of new conducting salts, dissolved in an organic solvent (PC or acetonitrile), for the preparation of advanced electrolytes [5]. The use of these salts allows the preparation of electrolytes with high conductivity and low viscosity. Furthermore, the EDLCs based on these electrolytes perform at voltages larger than 3V. Several

studies have been dedicated to different cations (phosphonium and quaternary ammonium-based cations) combined mainly with tetrafluoroborate (BF_4^-) as anion. Recently, pyrrolidinium-based cations have appeared as promising candidates for the generation of advanced electrolytes [1,4]. Since the ions of the conducting salts are involved on the formation of electrical double layer, the selection of a conducting salt with adequate ion sizes, chemical and electrochemical stability is crucial for the development of advanced electrolytes [5].

Moreover, the appropriate selection of ions has a strong influence on the carbon-electrolyte interface [11–13]. To take full benefit from the advantages of innovative electrolytes, the physicochemical properties of carbon materials must be also carefully considered. In this sense, the effect of porous texture has been extensively analyzed in the literature when using non-conventional electrolytes. It has been proven that carbon materials with well-developed microporosity and adequate pore size distribution (with optimized ion size/pore size ratios) are highly desirable since they provide high specific capacitance [11–14]. However, other key parameters, such as the surface chemistry of carbon materials, has not been thoroughly discussed yet in these electrolytes, although its influence has been clearly proven in other media (aqueous and organic electrolytes). Specifically, doping with different heteroatoms (such as nitrogen) can improve several properties in aqueous and organic electrolyte, such as electrical conductivity, electrochemical stability, etc. Although several works have focused on the use of N-doped carbons as electrodes in ionic liquid-based electrolytes [15–22], the role of nitrogen functional groups on the electrochemical performance has not been extensively assessed yet. As discussed above, the performance of EDLC strongly depends on the interaction at the electrode-electrolyte interface. Thus, surface chemistry appears as a key parameter to be investigated for the development of EDLCs based in non-conventional electrolytes.

One of the main drawbacks when assessing the effect of heteroatom doping of carbon electrodes lies in the difficulties of controlling their physicochemical properties: porous texture and surface chemistry. For instance, the doping with nitrogen using the most usual protocols normally affect the porous texture of the carbon material and makes difficult to elucidate the role of different parameters in their electrochemical performance [23–25]. Ideally, the performance of heteroatom-doped carbons must be compared to that of a non-doped material with almost identical porous texture and morphology [23]. In this sense, we have developed

nitrogen-doped carbon materials by post-functionalization strategies under mild conditions that allow full preservation of the porous texture of the pristine carbon material, even when using activated carbons with well-developed microporosity [26] and seamless structure [27]. The comprehensive comparison of the physicochemical and electrochemical properties of the doped and non-doped carbons has been used as an appropriate approach to assess the role of surface chemistry in their performance as electrodes for supercapacitors in aqueous and organic electrolytes [26–28]. Thus, the study of the effect of this functionalization methods in the performance of these materials when using non-conventional electrolytes can be considered as an adequate strategy to study the carbon-electrolyte interface when using N-doped carbon materials and electrolytes based in ionic liquids and new conducting salts (in organic electrolyte).

In this work, the effect of nitrogen functionalization treatments on the electrochemical properties of the activated carbons with high surface area was analyzed using non-conventional electrolytes. For this, nitrogen functionalization is carried out throught chemical post-treatments at mild conditions over a superporous activated carbon with tailored porous structure. The effect of nitrogen functional groups on the electrochemical performance of the carbon materials is assessed in two PC-based electrolytes: (i) a non-conventional conducting salt (1-butyl-1-methylpyrrolidium tetrafluoroborate ($Pyr_{14}BF_4$)) in PC and (ii) a mixture of ionic liquid (1-butyl-1-methylpyrrolidium bis-(tri-fluoromethylsulfonyl)imide ($Pyr_{14}TFSI$)) with PC.

2. Materials and Methods

2.1. Activated carbon

A superporous activated carbon prepared in our laboratory has been used as the starting material for nitrogen incorporation via post-modification treatments based in organic chemistry reactions. The pristine material (named as KUA), has been obtained by chemical activation of a Spanish anthracite with KOH using an impregnation ratio of activating agent to raw material of 4:1 and an activation temperature of 750º C under inert atmosphere, which was held for 1 hour. More details about the preparation process are available elsewhere [29] [18].

2.2. Chemical functionalization of activated carbon

KUA was further functionalized with nitrogen functional groups by two different strategies based on the organic chemistry protocols. This methodology was accurately described in the literature [26,30]. Briefly, the first approach consisted in a three-step protocol with the aim to attach amide functionalities on the activated carbon KUA. The treatment was carried out as follows:

(i) Chemical oxidation with HNO_3 to produce oxygen functional groups (activated carbon to solution ratio of 1g/40 mL).

(ii) Generation of acyl chloride functionalities by reaction of the oxidized activated carbon with $SOCl_2$ in toluene under Ar atmosphere (activated carbon to solution ratio of 1g/55mL)

(iii) Amidation reaction over the activated carbon produced in step (ii) with 2M NH_4NO_3/DMF solution and pyridine (activated carbon to solution ratio of 1g/300mL).

The obtained sample was named as KUA-$CONH_2$. In the second method, the third step of the first protocol is directly applied over pristine sample (KUA), thus avoiding any oxidation treatment. This sample was named as KUA-N.

2.3. Porous texture and surface chemistry characterization

The porous texture characterization was carried out by N_2 adsorption-desorption isotherms at -196º C and by CO_2 adsorption at 0º C by using an Autosorb-6-Quantachrome apparatus. The samples were outgassed at 200º C for 4 hours before the experiments. The apparent surface area was obtained from N_2 adsorption isotherms by using the BET equation in the 0.05-0.20 range of relative pressures. The total micropore volume was determined by Dubinin-Radushkevich (DR) method applied to N_2 (relative pressures from 0.01 to 0.05) adsorption isotherms. The volume of the narrow microporosity (i.e., pore sizes below 0.7 nm) was calculated from the DR method applied to the CO_2 adsorption isotherms (relative pressures from 0.0001 to 0.25) [31]. The pore size distributions (PSD) for the materials have been calculated from the N_2 adsorption isotherms using NL-DFT method as proposed by Jagiello and Olivier [32] using SAIEUS© software.

The surface chemistry of the samples was analyzed by X Ray Photoelectron Spectroscopy (XPS) and Temperature Programmed Desorption (TPD). XPS measurements were performed by using a VG-Microtech Multilab 3000 spectrometer, equipped with an Al anode. TPD experiments were performed by heating the samples (~10 mg) to 950º C (at a heating rate of 20º C/min) under a helium flow rate of 100 mL/min. The analyses were carried out by using a TGA-DSC instrument (TA Instruments, SDT Q600 Simultaneous) coupled to a mass spectrometer (Thermostar, Balzers, BSC 200). The samples were also characterized by Scanning Electron Microscopy (SEM) coupled to Energy Dispersive X-Ray Analysis (EDX) by using a Hitachi equipment, S3000N model.

2.4. Electrolyte preparation

Two different electrolytes were employed in this work: 1M $Pyr_{14}TFSI$/PC and 1M $Pyr_{14}BF_4$/PC. The IL $Pyr_{14}TFSI$ (IoLiTec, 99.5%) was dried by using a molecular sieve until the water content was lower than 20 ppm. The conducting salt $Pyr_{14}BF_4$ was purified as described elsewhere [33]. PC (Sigma Aldrich, 99.7 %) was used as organic solvent. The water content of the electrolytes was determined to be lower than 30 ppm, as measured by Karl-Fisher technique.

2.5 Electrochemical characterization

2.5.1. Three electrode cell configuration

The electrochemical characterization of the carbon materials was performed by using a Swagelock-type cell in a three-electrode configuration. The working electrodes were prepared by mixing the activated carbon with acetylene black and polytetrafluoroethylene (PTFE) as binder in a ratio of 85:10:5 (w/w). The total weight of the electrode was ~4-5 mg (dry basis). For shaping the electrodes, a sample sheet was cut into a circular shape with an area of 0.95 cm^2. The counter electrodes were prepared using a commercial activated carbon as active material (Norit DLC Super30, S_{BET} = 1618 m^2/g) with a mass loading larger than 30 mg/cm^2, as described elsewhere [14]. The electrodes were dried overnight at 120 ºC under vacuum prior to assembling the cell.

The cells were prepared inside an Ar-filled glovebox with water and oxygen contents < 1 ppm. The working and counter electrodes were tightly pressed against each other and separated by a glass microfiber membrane (Whatman GF/D, thickness: 675 µm). Prior to assembling the cell, the separator and the electrodes were soaked with 140 µL of electrolyte and kept under vacuum for 5 minutes. Ag was used as reference electrode in all cases.

The electrochemical characterization of all samples was tested by CV at sweep rate of 1 mV/s. The capacitance was calculated from the electric charge of the CV. The results are expressed in F/g, considering the weight of the active material of the working electrode.

2.5.2. EDLC investigation.

Asymmetric in mass EDLC were assembled for all carbon materials in an Argon glovebox in 1M $PYR_{14}TFSI$/PC electrolyte. For this, two electrodes (surface area: 0.283 cm^2) were prepared with a weight of ~1.1 mg (active phase) each. Supercapacitors were constructed by pressing both electrodes against each other and separating them by a filter glass microfiber membrane (Whatman GF/D, thickness: 675 µm). These devices were characterized by CV at different scan rates and galvanostatic charge-discharge (GCD) cycles at current densities from 1 to 20 A/g in 1M $PYR_{14}TFSI$/PC. CV measurements were performed in a Biologic VSP 300 and the galvanostatic tests in a Arbin SCTS galvanostat. Electrochemical Impedance Spectroscopy (EIS) were perforded at 0.05V in the frequency range of 10mHz-100 kHz with an amplitude voltage of 10 mV by using an Autolab PGSTAT302 potentiostat. A durability test for asymmetric capacitors was performed by 2000 GCD cycles at a current density of 1 A/g and a voltage of 3.0 V. Current density and specific capacitance is defined based on the total active weight of the carbon material included in both electrodes. Volumetric capacitance was calculated using the electrode density.

The energy density and power density of asymmetric supercapacitors was calculated in order to obtain all relevant information about their performance. Energy density was obtained during the discharge cycle from 3 to 0 V by the following equation (1):

$$E = \int_0^Q V dQ \qquad (1)$$

Where Q is the total charge measured during the discharge step (C), V is the cut-off voltage (V) and w is the active phase of the electrodes (g).

Power density was calculated according to equation (2):

$$P = \frac{E}{t_d} \quad (2)$$

Where t_d is the time of discharge in the GCD cycle.

3. Results and Discussion

3.1 Surface chemistry and porous texture characterization

Table 1 summarizes the main parameters related to the physicochemical properties of the pristine and N-functionalized activated carbons. These properties and the effect of nitrogen doping on the surface chemistry and porous texture of the samples has been previously discussed [26,30] and are summarized below. As evidenced by XPS analyses, nitrogen doping was satisfactorily achieved for KUA-N and KUA-$CONH_2$ samples through consumption of oxygen functionalities. Both N-doped carbons show similar nitrogen spectra and content (~ 4 at. % XPS), but the functionalities generated on their surfaces are different. This is a consequence of the different oxygen functional groups involved in the reaction. For the production of KUA-N sample, the nitrogen doping is carried out directly over the pristine carbon material; as a result, the nitrogen functionalities generated on this carbon are derived mainly from CO-evolving groups. Thus, the main functional groups found over this carbon material are amines, pyridines/imines and pyrroles/pyridones [26]. Nevertheless, the nitrogen functional groups produced on KUA-$CONH_2$ involve the consumption of CO_2 and CO evolving-groups, since the pristine carbon was previously oxidized to increase the oxygen content prior to the nitrogen doping step. Hence, there is a contribution of groups derived from CO_2 (amide-like functionalities) and CO groups (pyridines, pyrroles, etc.) [30]. Consequently, the N-doped carbons show similar nitrogen content, but different surface functionalities. Also, KUA-$CONH_2$ has a larger amount of oxygen functional groups than the other carbons.

Table 1. Surface composition determined for all activated carbons by XPS and TPD.

Sample	C_{XPS} (at. %)	N_{XPS} (at.%)	O_{XPS} (at.%)	$CO_{2\ TPD}$ (µmol/g)	CO_{TPD} (µmol/g)	O_{TPD} (µmol/g)

KUA	90.9	0.3	8.8	500	2100	3100
KUA-N	87.6	3.6	8.8	450	1750	2640
KUA-CONH$_2$	88.8	4.1	12.0	1140	2370	4650

The porous texture of the samples was assessed by N_2 and CO_2 adsorption isotherms. Figure 1 includes the N_2 adsorption isotherms of the materials as well as the pore size distributions calculated from the NL-DFT method. The pristine carbon material is a microporous material with high apparent surface area [26]. Moreover, most of the microporosity of the pristine material remains in the N-doped samples due to the mild conditions of the treatment. When the nitrogen doping is carried out directly over the pristine carbon (KUA-N sample), the microporosity is fully preserved since only chemical reactions involving CO groups take place to attach nitrogen moieties. However, KUA-CONH$_2$ evidences some loss of the microporosity (30 %) mainly due to the oxidation pre-treatment done prior to the nitrogen functionalization treatment [30].

Table 2. Porous texture parameters of the activated carbons.

Sample	**S_{BET} (m^2/g)**	**V_{DR}^{N2} (cm^3/g)**	**V_{DR}^{CO2} (cm^3/g)**
KUA	3080	1.19	0.57
KUA-N	2960	1.18	0.52
KUA-CONH$_2$	2390	0.97	0.45

The sample KUA shows a wide micropore size distribution, with an average pore size of 1.4 nm (Figure 1b). The nitrogen doping does not significantly modify the pore size distribution in the case of sample KUA-CONH$_2$. However, an increase in the region of micropores of size below 1 nm is detected in the case of sample KUA-N. Thus, nitrogen doping at mild conditions allows the generation of carbon materials with similar porous texture but different functionalities.

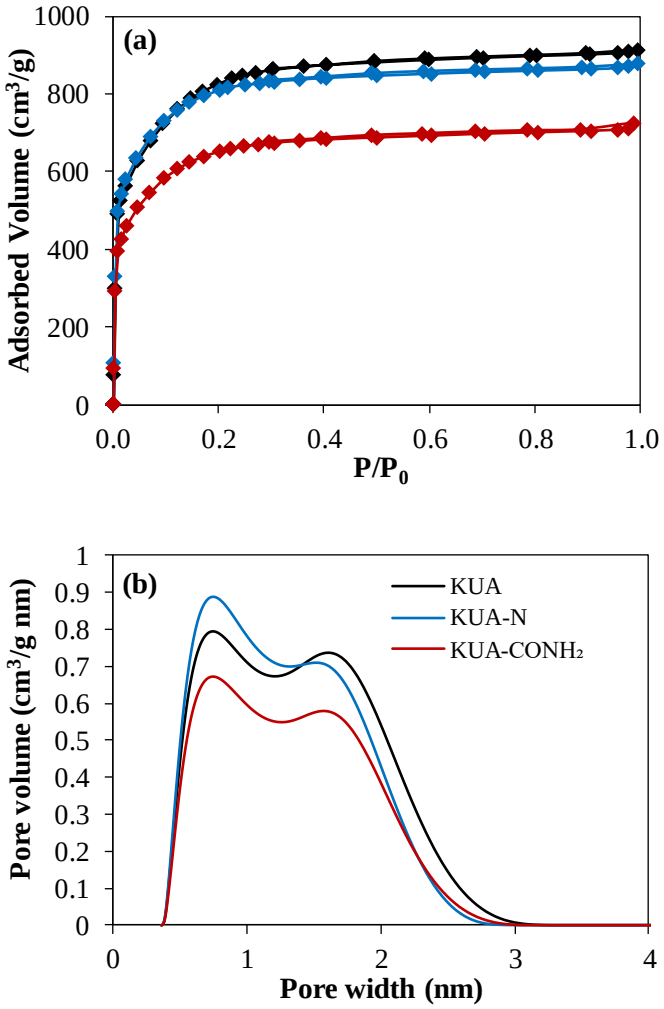

Figure 1. (a) N_2 adsorption desorption isotherms and (b) Differential pore size distributions obtained by NL-DFT calculations of KUA, KUA-N and KUA-$CONH_2$.

3.2 Electrochemical characterization

3.2.1 Three-electrode cell configuration

The electrochemical performance of the samples was tested by cyclic voltammetry in three-electrode cells in 1M Pyr_{14}TFSI/PC and 1M $Pyr_{14}BF_4$/PC. The CVs were recorded from the open circuit potential (E_{OCP}) upon negative and positive potential (each side was investigated using fresch cells), by broadening 0.10 V the potential limit of every cycle with respect to the previous one. Figure 2 shows the selected CVs when approaching the stability limits under negative (figure 2a) and positive (figure 2b) polarization for the three activated carbons in 1M $Pyr_{14}BF_4$/PC electrolyte. More selected CVs are presented at the Supplementary Data (figure

S1). The pristine activated carbon (KUA) displays faradaic processes under conditions of negative polarization. A cathodic current is recorded starting at -1.70 V, with the corresponding reverse anodic peak at -0.30 V. These faradaic charge transfer reactions can be associated to oxygen functionalities and partial decomposition of PC [14,34–36]. At positive polarization, redox processes are observed at 1.0 V, and an anodic current starts at 1.2 V evidencing the occurrence of oxidation processes.

The CVs clearly evidence than nitrogen doping affects the electrochemical performance of the activated carbons. First, the N-doped carbons (KUA-N and KUA-$CONH_2$) display lower E_{OCP} than the parent non-doped carbon, indicating that the generation of nitrogen functionalities modifies the carbon-ion interaction during non-charging regime [37]. Moreover, the nitrogen doping affects the electrochemical stability of the carbon materials. At negative polarization from the open circuit potential, both samples present a faradaic process at -1.70 V. However, the current values reached during the reverse scan are much lower than those of the non-doped carbon, highlighting the higher stability of the N-doped carbons. Furthermore, the N-doped carbons show a CV with a square shape among the whole potential range, evidencing an ideal EDLC behavior even at potentials close to the limit value of stability.

Similar features are observed at the positive potential range (Figure 2b). The lower E_{OCP} detected for the N-doped carbons provides a wider potential window upon positive polarization. Thus, the symmetric configuration in supercapacitor cells using these materials might provide higher durability, since a better balance of the charge is expected during the operation of the device. Moreover, at high positive potentials (> 1.2 V), the faradaic current detected for the N-doped carbon materials is considerably lower than the one exhibited by KUA, as confirmed also by the values of coulombic efficiency calculated under these conditions (86, 98 and 98% for KUA, KUA-N and KUA-$CONH_2$ electrodes, respectively). The lower occurrence of faradaic processes indicates an improvement of electrochemical stability under oxidative conditions that can be associated to the formation of nitrogen groups. More details about the performance of the samples under positive polarization can be observed in Figure S1.

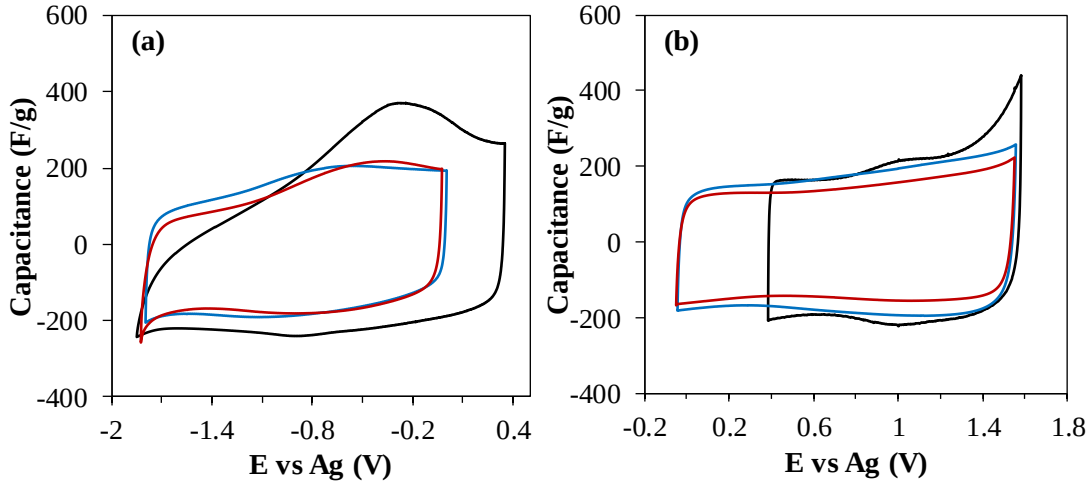

Figure 2. Cyclic voltammograms obtained for KUA (black), KUA-N (blue) and KUA-$CONH_2$ (red) electrodes in (a) negative and (b) positive potential ranges. 1M $Pyr_{14}BF_4$/PC. v = 1 mV/s.

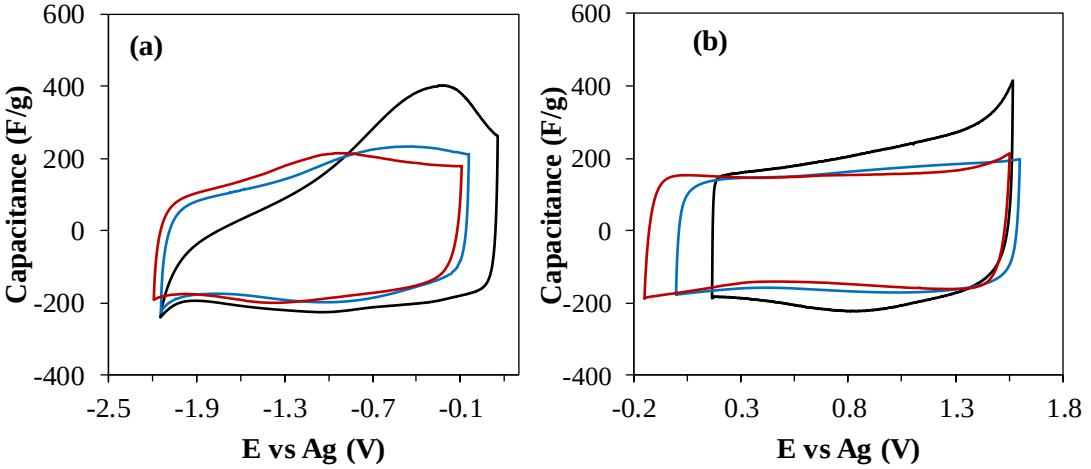

Figure 3. Cyclic voltammograms obtained for KUA (black), KUA-N (blue) and KUA-$CONH_2$ (red) electrodes in (a) negative and (b) positive potential ranges. 1M Pyr_{14}TFSI/PC. v = 1 mV/s.

The potential window of the carbon materials was also analyzed by CV in 1M Pyr_{14}TFSI/PC. More details about the polarization processes can be observed in figure S2 at the Supplementary Data. As detected in 1M $Pyr_{14}BF_4$/PC, the carbon electrodes exhibit a cathodic current related to decomposition processes. However, in this case the faradaic current is detected at more negative potentials (- 2.0 V), evidencing a larger electrochemical stability window in case of the IL mixture. Under conditions of positive polarization, KUA exhibits larger faradaic currents when increasing the potential, evindencing lower electrochemical stability also in this electrolyte. Furthermore, KUA-$CONH_2$ electrode displays an increase of

faradaic cathodic current at 1.5 V, that is not observed in case of KUA-N electrode, evidencing lower electrochemical stability for the former than for the latter.

Even though surface chemistry influences the electrochemical stability of the carbon materials in the electrolytes, all of them display larger electrochemical stability window in IL-based electrolyte than in the other electrolyte. This result is in agreement with the performance of other carbons in the literature [11,13,38,39].

The gravimetric capacitance was determined using a potential window in absence of faradaic contributions (figures S1 and S2, green curves). Table 3 collects the values obtained under positive (C_+) and negative (C_-) polarization in both electrolytes. However, it should be remarked that C_+ and C_- cannot be exclusively associated to adsorption of anions and cations, respectively. Several studies have demonstrated that the charge storage in supercapacitors is not produced by single electrosorption of ions on the surface of the charged electrode. The formation of the electrical double layer (EDL)can be produced by different mechanisms depending on the electrolyte and the electrode, as well as the electrode polarization [40,41]. Independently of the mechanism governed in the formation of the EDL, the relative pore/ion size is a key parameter to be considered [13,14,42,43], since the ions might diffuse across the pore network involved in the charging process.

The pristine activated carbon displays extraordinary capacitance values in both electrolytes due to its tailored porous texture, which has been optimized to be used in these electrolytes. [14]. Even though 1M $Pyr_{14}TFSI$/PC shows higher viscosity than 1M $Pyr_{14}BF_4$/PC (Table 4), both electrolytes provide large capacitance values when using KUA as electrode material. The main differences in terms of capacitance are a consequence of the different sizes of the ions: 0.46 nm (BF_4^-), 0.79 nm ($TFSI^-$) and 1.1 nm (Pyr_{14}^+) [11,44]. On the other hand, KUA has a large micropore volume and an average pore size of 1.4 nm. Hence, KUA provides an adequate pore size distribution to allow the diffusion of the electrolyte-containing ions to its inner surface.

The N-doped activated carbons show slightly lower capacitance values in both electrolytes, indicating that nitrogen doping does not improve the formation of the EDL in these electrolytes. Several studies have pointed out the beneficial effect of nitrogen functional groups in terms of

capacitance in aqueous and organic electrolyte [45–47]. However, the contribution of the different N moieties in organic and ionic liquid-based electrolytes is not straightforward. Oschazt et al. reported that nitrogen functional groups do not contribute to the increase of capacitance [20], which is in agreement with our results. Moreover, these carbon materials show a very well developed microporosity, and consequently the large apparent surface area could minimize the contribution of nitrogen groups in the formation of the EDL. Thus, the differences in the capacitance values can be explained by the small losses of microporosity produced during the functionalization treatment. KUA-N evidenced a small modification of porous texture. However, the ions of the electrolytes have large sizes, and consequently small changes on the pore width might affect the formation of the EDL. Thus, the differences in capacitance might arise from the small modification of the pore size distribution in these samples (see Figure 1b), as well as the slightly lower available surface area. Since BF_4^- anion is smaller than $TFSI^-$, it can have access to smaller micropores. Hence, the higher capacitance values detected in 1M $Pyr_{14}BF_4$/PC for KUA-N in the positive potential window, can be a consequence of the significant increase of micropores of size lower than 1nm observed after functionalization in this sample. More interesting features are observed for KUA-$CONH_2$ activated carbon. This sample displays similar capacitance values in 1M $Pyr_{14}TFSI$/PC than KUA-N, but lower values in 1M $Pyr_{14}BF_4$/PC. Since KUA-$CONH_2$ shows lower micropore volume than KUA-N, the formation of EDL in the IL-based electrolyte might not involve the whole microporosity of both carbons, but only a range of micropores that contain both carbon materials. In addition, some effect of the surface chemistry cannot be discarded.

Table 3. Gravimetric capacitance calculated for the carbon electrodes in the electrolytes in different potential ranges.

Sample	**1 M $Pyr_{14}BF_4$/PC**		**1M $Pyr_{14}TFSI$/PC**	
	C_+ (F/g)	**C_-(F/g)**	**C_+ (F/g)**	**C_-(F/g)**
KUA	187	185	168	193
KUA-N	165	161	153	163
KUA-$CONH_2$	147	153	157	165

Table 4. Viscosity and conductivity of the electrolytes at 20 ºC [11].

Electrolyte	Viscosity (mPa s)	Conductivity (mS/cm)
1M $Pyr_{14}BF_4$/PC	4.2	9.8
1M Pyr_{14}TFSI/PC	5.1	7.3

3.2.2 EDLC investigation

Asymmetric EDLCs (in mass) were assembled to evaluate the performance of the carbon electrodes at high operation voltage (3 V) in 1M Pyr_{14}TFSI/PC. The mass loading of the carbon materials was balanced by following the methodology proposed by Peng et al. [48]. By following this strategy, the performance of the EDLC can be enhanced and the premature ageing of cells should be avoided. For this, the capacitance values were determined in the electrochemical stability windows determined in section 3.2.1. The mass ratio was calculated by using the equation (3):

$$w_+/w_- = C_{g\_} \cdot |\Delta V_-|/(C_{g_+} \cdot \Delta V_+) \quad (3)$$

Where w_+/w_- is the mass ratio of the electrodes, C_{g+} and C_{g-} are the capacitance values under positive and negative polarization, and ΔV_+ and ΔV_- are the positive and negative windows, respectively.

Figure 4a shows the CV obtained for the three activated carbon-based EDLCs at 20 mV/s. The devices display an ideal rectangular shape, characteristic of electrical double layer, and provide large capacitance values (37-40 F/g). The lowest value was determined for KUA-$CONH_2$ as consequence of its lower porosity. Figure 4b illustrates the evolution of capacitance when increasing the scan rate. The capacitors provide high retention of capacitance at large scan rates, demostrating values of ~ 20 F/g at 500 mV/s. The capacitors based on KUA-N and KUA-$CONH_2$ supply slighly higher retention of capacitance, as happened in aqueous [26,30] and organic electrolytes [28]. These results are in agreement with the Nyquist plots obtained for the devices (see figure S3). The improvement of capacitance retention in all media might be undoubtely related to an enhancement of electrical conductivity due to the substitution of electron-withdrawing oxygen functional groups with electron-donor nitrogen functionalities [28].

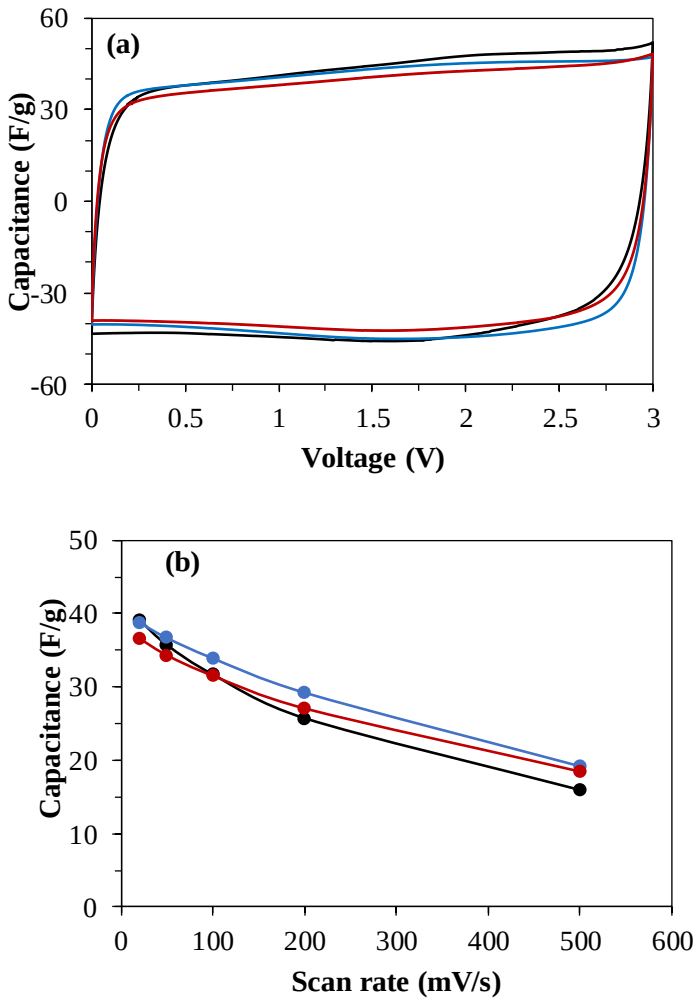

Figure 4. (a) Cyclic voltammograms obtained for KUA (black), KUA-N (blue) and KUA-$CONH_2$ (red) based capacitors. v = 20 mV/s. (b) Evolution of capacitance with the scan rate (20, 50, 100, 200 and 500 mV/s). 1M Pyr_{14}TFSI/PC.

The performance of the capacitors was analyzed using a cycling test at different current densities. Figure 5 illustrates the GCD cycles and the Ragone plot obtained for the EDLCs. Table 5 collects the parameters of the devices obtained from the cycling test. The gravimetric capacitance values are among the largest reported in the literature in IL-based electrolytes [17–19,22,49,50]. Furthermore, the devices show outstanding performance in terms of volumetric capacitance since the carbon electrodes contain almost negligible mesoporosity, which is commonly used to enhance the performance in ILs [17,18,22,50,51](not reported in these references). Hence, the combination of highly microporous activated carbons with IL-based

electrolytes allows the production of devices with excellent energy densities in gravimetric and volumetric basis (44-48 Wh/kg and 16-17 Wh/L, respectively, Table 5).

Moreover, the N-doped carbon-based EDLCs evidence larger coulombic and energy efficiency than the pristine KUA-based capacitor, providing better reversibility of the N-doped samples upon cycling. This must be related to the lower occurrence of faradaic processes, as discussed in section 3.2.1. Thus, the generation of stable nitrogen functionalities, as well as the decrease of detrimental oxygen groups, enhance the electrochemical performance of carbon electrodes, as happened in organic and aqueous electrolytes.

Table 5. Gravimetric capacitance (C_g), volumetric capacitance (C_v), specific energy (E_g), energy density (E_v), coulombic efficiency and energy efficiency determined for KUA, KUA-$CONH_2$ and KUA-N asymmetric supercapacitors at the voltage 3V by GCD cycles. 1M Pyr_{14}TFSI/PC. j=1 A/g.

Sample	C_g (F/g)	C_v (F/cm^3)	E_g (Wh/Kg)	E_v (Wh/L)	Coulombic efficiency (%)	Energy efficiency (%)
KUA	40	14	46	16	99	84
KUA-N	40	14	48	17	100	89
KUA-$CONH_2$	37	14	44	16	100	87

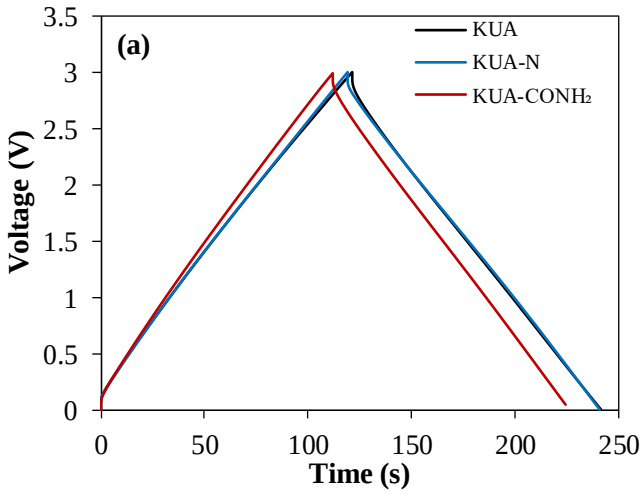

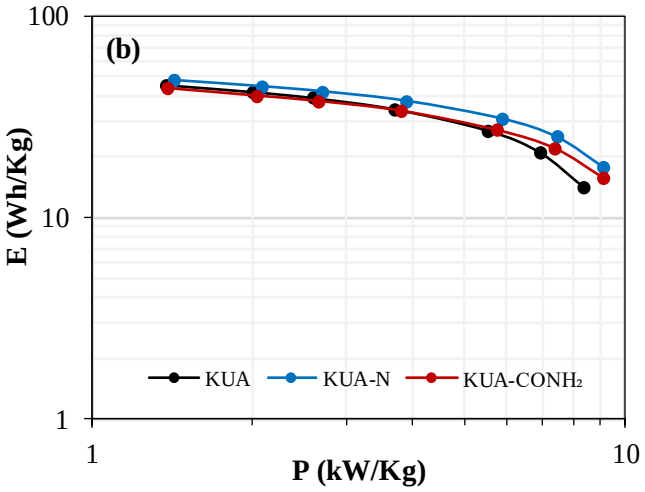

Figure 5. (a) Galvanostatic charge-discharge cycles for KUA, KUA-N and KUA-$CONH_2$ asymmetric supercapacitors at 3V and 1A/g. (b) Ragone plot at 3V for all asymmetric supercapacitors. j = 1-10 A/g. 1M Pyr_{14}TFSI/PC.

Figure 5 illustrates the Ragone plot obtained for all activated carbon-based capacitors in 1M Pyr_{14}TFSI/PC. At low specific power (1.5 kW/kg), the cells provide similar specific energy values (44-48 Wh/kg, Table 5). However, the N-doped carbon-based EDLCs can keep higher values when increasing the specific power up to 9 kW/kg (14Wh/kg for KUA, and 15-18 Wh/kg for the N-doped activated carbon-based capacitors). This is related to the improvement of conductivity produced by the nitrogen functional groups [26,30,52,53] and the enhancement of ion dynamics due to the beneficial interaction between IL ions and N moieties [20].

The durability of the capacitors has been made carrying out 5000 GCD cycles at 3 V. Figure 6 shows the evolution of capacitance along cycles for the EDLCs containing non-doped and N-doped carbon electrodes.The non-doped carbon-based EDLC keeps the initial capacitance during the first thousand cycles, and afterwards it experiences a remarkable loss of capacitance and only retains around 60% of the initial capacitance after the durability test. A similar trend is observed for KUA-$CONH_2$ based EDLC, which evidences a strong loss of capacitance during the cyclability test. However, the EDLC based on KUA-N carbon exhibits a stable performance along cycles, providing a capacitance retention of 90 % after the durability test. This improvement might be undoubtedly related to the lower occurrence of faradaic reactions during the charge-discharge process, that lead to the degradation of the electrodes and electrolytes [34,36]. Since the materials employed in the construction of the cells have very similar porous

texture, the differences on the performance might be related to the modifications on the surface chemistry produced by the nitrogen doping treatment. Interestingly, only the capacitor based on KUA-N sample evidences an improvement on the electrochemical stability. This improvement might be associated to the reduction of detrimental oxygen functional groups [34] as well as the generation of nitrogen groups with higher electrochemical stability [26,45]. The poor performance of KUA-$CONH_2$ based EDLC can be a consequence of the pre-oxidation treatment carried out in the doping treatment, since it produces CO and CO_2-evolving groups that are detrimental for the electrochemical stability of carbon electrodes. Moreover, the N functional groups of this carbon electrode (mainly amide-like functional groups) do not mitigate the detrimental effect of oxygen surface groups, as has been proven to occur in pure PC-based organic electrolyte [28]. Thus, the surface functionalities generated on KUA-$CONH_2$ might be detrimental when using Pyr_{14}TFSI as electrolyte (either pure or as mixture).

To deepen into the degradation of the electrodes during the operation of the devices, the morphology of the electrodes was analyzed by SEM-EDX (before and after cycling). The SEM images and the surface composition are collected in the SI (see figures S4-6 and table S1). The results evidenced that the most important changes happen in the negative electrodes for all cells, mainly caused by the precipitation of the salts present in the electrolyte. Moreover, an increase of oxygen content was also observed in the positive electrodes. The lowest alteration of the surface composition was observed for KUA-N electrodes.

Hence, the results evidence that nitrogen doping can improve the durability of carbon electrodes when tested in IL-based EDLCs. However, the formation of selective nitrogen functional groups has a strong influence on the performance of the carbon material. Particularly, the generation of heterocycles and amine-like functional groups, in combination with a minimal presence of oxygen functional groups, are key parameters for improving the carbon performance as electrodes for supercapacitors in IL-based electrolytes. Thus, the functionalization used for the production of KUA-N is specially interesting as post-treatment for purification of carbon materials for their use in supercapacitors, since improves the electrochemical stability avoiding the loss of porosity (and capacitance) that often occurs in conventional processes that involve thermal treatments.

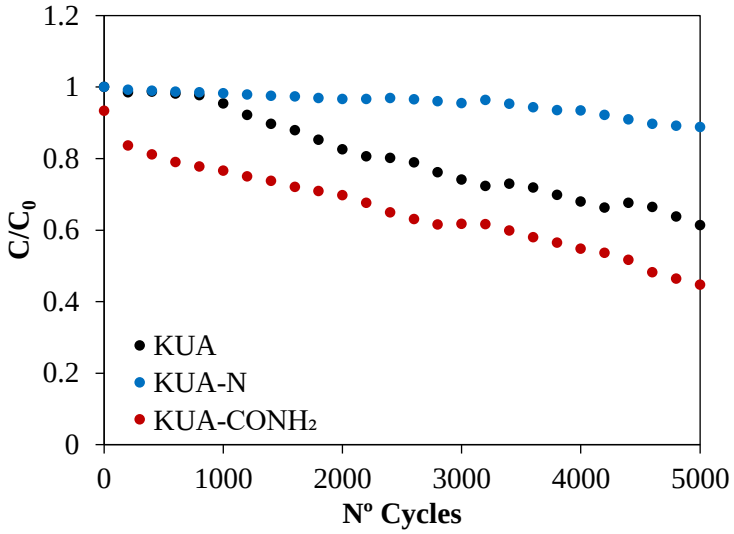

Figure 6. Cyclability test for KUA, KUA-N and KUA-$CONH_2$ based supercapacitors at 3V. j = 2A/g. 5000 cycles. 1M Pyr_{14}TFSI/PC.

4 Conclusions

In this work, the effect of nitrogen functionalization at mild conditions on the electrochemical performance of activated carbons in non-conventional electrolytes was studied. The generation of nitrogen functionalities at low temperature allows the preservation of most of the tailored porous texture of the pristine carbon material, which is crucial for the development of EDLCs based in innovative electrolytes.

The electrochemical characterization of the samples in two different electrolytes, with the same cation but different anion, allows to elucidate the different parameters affecting the electrode-electrolyte interface. It was found that surface chemistry does not significantly modifies the capacitance, but has a strong effect on the degradation of both electrodes and electrolytes. The nitrogen doping decreases the degradation processes occurring in the carbon electrodes under positive and negative polarization, when approaching the limits of the electrochemical stability window.

Supercapacitors based on these activated carbons in IL-based electrolyte displayed very high capacitance (37-40 F/g and 14 F/cm^3) and energy densities (44-48 Wh/kg and 16-17 Wh/L), with improved rate performance as consequence of the generation of nitrogen functional groups. The effect of nitrogen doping on the durability of the devices was analysed by a cycling

test. The results evidenced that the formation of selective N functional groups can produce a remarkable improvement of the electrochemical stability of carbon materials when working as electrodes in IL-based EDLCs. This effect is associated to the decrease of the amount of oxygen functional groups, as well as the generation of N functional groups with high electrochemical stability and good affinity with the IL-based electrolyte. The doping method at mild conditions used on this work is especially interesting since avoids the loss of surface porosity, and consequently does not compromise other supercapacitor properties, such as capacitance and energy density.

Acknowledments. The authors thank MICINN, FEDER (RTI2018-095291-B-I00 and ENE2017-90932-REDT). MJML acknowledges financial support through VALi+d grant (ACIF/2015/374) and mobility grant (BEFPI/2017/036).

References

[1] F. Béguin, V. Presser, A. Balducci, E. Frackowiak, Carbons and electrolytes for advanced supercapacitors, Adv. Mater. 26 (2014). doi:10.1002/adma.201304137.

[2] W. Raza, F. Ali, N. Raza, Y. Luo, K.H. Kim, J. Yang, S. Kumar, A. Mehmood, E.E. Kwon, Recent advancements in supercapacitor technology, Nano Energy. 52 (2018) 441–473. doi:10.1016/j.nanoen.2018.08.013.

[3] P. Simon, Y. Gogotsi, Materials for electrochemical capacitors., Nat. Mater. 7 (2008) 845–54. doi:10.1038/nmat2297.

[4] C. Zhong, Y. Deng, W. Hu, J. Qiao, L. Zhang, J. Zhang, A review of electrolyte materials and compositions for electrochemical supercapacitors, Chem. Soc. Rev. 44 (2015) 7484–7539. doi:10.1039/c5cs00303b.

[5] A. Balducci, Electrolytes for high voltage electrochemical double layer capacitors: A perspective article, J. Power Sources. 326 (2016) 534–540. doi:10.1016/j.jpowsour.2016.05.029.

[6] J. Krummacher, C. Schütter, L.H. Hess, A. Balducci, Non-aqueous electrolytes for electrochemical capacitors, Curr. Opin. Electrochem. 9 (2018) 64–69. doi:10.1016/J.COELEC.2018.03.036.

[7] A. Brandt, S. Pohlmann, A. Varzi, A. Balducci, S. Passerini, Ionic liquids in supercapacitors, MRS Bull. 38 (2013) 554–559. doi:10.1557/mrs.2013.151.

[8] D.R. Macfarlane, N. Tachikawa, M. Forsyth, J.M. Pringle, P.C. Howlett, G.D. Elliott, J.H. Davis, M. Watanabe, P. Simon, C.A. Angell, Energy applications of ionic liquids, Energy Environ. Sci. 7 (2014) 232–250. doi:10.1039/c3ee42099j.

[9] W.Y. Tsai, R. Lin, S. Murali, L. Li Zhang, J.K. McDonough, R.S. Ruoff, P.L. Taberna, Y. Gogotsi, P. Simon, Outstanding performance of activated graphene based supercapacitors in ionic liquid electrolyte from -50 to 80°C, Nano Energy. 2 (2013) 403–411. doi:10.1016/j.nanoen.2012.11.006.

[10] V.L. Martins, R.M. Torresi, Ionic liquids in electrochemical energy storage, Curr. Opin. Electrochem. 9 (2018) 26–32.

[11] S. Pohlmann, R.S. Kühnel, T.A. Centeno, A. Balducci, The Influence of Anion-Cation Combinations on the Physicochemical Properties of Advanced Electrolytes for Supercapacitors and the Capacitance of Activated Carbons, ChemElectroChem. 1 (2014) 1301–1311. doi:10.1002/celc.201402091.

[12] S. Pohlmann, C. Ramirez-Castro, A. Balducci, The Influence of Conductive Salt Ion Selection on EDLC Electrolyte Characteristics and Carbon-Electrolyte Interaction, J. Electrochem. Soc. 162 (2015) A5020–A5030. doi:10.1149/2.0041505jes.

[13] S. Pohlmann, B. Lobato, T.A. Centeno, A. Balducci, The influence of pore size and surface area of activated carbons on the performance of ionic liquid based supercapacitors, Phys. Chem. Chem. Phys. 15 (2013) 17287–17294. doi:10.1039/c3cp52909f.

[14] S. Leyva-García, D. Lozano-Castelló, E. Morallón, T. Vogl, C. Schütter, S. Passerini, A. Balducci, D. Cazorla-Amorós, Electrochemical performance of a superporous activated carbon in ionic liquid-based electrolytes, J. Power Sources. 336 (2016) 419–426. doi:10.1016/j.jpowsour.2016.11.010.

[15] A.S. J.-K. Ewert, D. Weingarth, C. Denner, M. Friedrich, M. Zeiger, R.K. N. Jäckel, V. Presser, Enhanced capacitance of nitrogen-doped hierarchically porous carbide-derived carbon in matched ionic liquids, J. Mater. Chem. 3 (2015) 18906–18912. doi:10.1039/c5ta04773k.

[16] D. Liu, C. Zeng, D. Qu, H. Tang, Y. Li, B.-L. Su, D. Qu, Highly efficient synthesis of ordered nitrogen-doped mesoporous carbons with tunable properties and its application in high performance supercapacitors, J. Power Sources. 321 (2016) 143–154. doi:10.1016/j.jpowsour.2016.04.129.

[17] M. Sevilla, G.A. Ferrero, N. Diez, A.B. Fuertes, One-step synthesis of ultra-high surface area nanoporous carbons and their application for electrochemical energy storage, Carbon. 131 (2018) 193–200. doi:10.1016/j.carbon.2018.02.021.

[18] A.B. Fuertes, M. Sevilla, High-surface area carbons from renewable sources with a bimodal micro-mesoporosity for high-performance ionic liquid-based supercapacitors, Carbon. 94 (2015) 41–52. doi:10.1016/j.carbon.2015.06.028.

[19] Y. Zheng, H. Wang, S. Sun, G. Lu, H. Liu, M. Huang, J. Shi, W. Liu, H. Li, Sustainable nitrogen-doped carbon electrodes for use in high-performance supercapacitors and Li-ion capacitors, Sustain. Energy Fuels. 4 (2020) 1789–1800. doi:10.1039/c9se01064e.

[20] R. Yan, M. Antonietti, M. Oschatz, Toward the Experimental Understanding of the Energy Storage Mechanism and Ion Dynamics in Ionic Liquid Based Supercapacitors, Adv. Energy Mater. (2018) 1800026. doi:10.1002/aenm.201800026.

[21] W. Tian, Q. Gao, L. Zhang, C. Yang, Z. Li, Y. Tan, W. Qian, H. Zhang, Renewable graphene-like nitrogen-doped carbon nanosheets as supercapacitor electrodes with integrated high energy–power properties, J. Mater. Chem. A. 4 (2016) 8690–8699. doi:10.1039/C6TA02828D.

[22] S.W. Xu, Y.Q. Zhao, Y.X. Xu, Q.H. Chen, G.Q. Zhang, Q.Q. Xu, D.D. Zhao, X. Zhang, C.L. Xu, Heteroatom doped porous carbon sheets derived from protein-rich wheat gluten for supercapacitors: The synergistic effect of pore properties and heteroatom on the electrochemical performance in different electrolytes, J. Power Sources. 401 (2018) 375–385. doi:10.1016/j.jpowsour.2018.09.012.

[23] A. Castro-Muñiz, Y. Hoshikawa, T. Kasukabe, H. Komiyama, T. Kyotani, Real Understanding of the Nitrogen-Doping Effect on the Electrochemical Performance of Carbon Materials by Using Carbon-Coated Mesoporous Silica as a Model Material, Langmuir. 32 (2016) 2127–2135. doi:10.1021/acs.langmuir.5b03667.

[24] Y. Deng, Y. Xie, K. Zou, X. Ji, Review on recent advances in nitrogen-doped carbons: Preparations and applications in supercapacitors, J. Mater. Chem. A. 4 (2015) 1144–1173. doi:10.1039/c5ta08620e.

[25] W. Shen, W. Fan, Nitrogen-containing porous carbons: synthesis and application, J. Mater. Chem. A. 1 (2013) 999–1013. doi:10.1039/c2ta00028h.

[26] M.J. Mostazo-López, R. Ruiz-rosas, E. Morallón, D. Cazorla-Amorós, Nitrogen doped superporous carbon prepared by a mild method. Enhancement of supercapacitor performance, Int. J. Hydrogen Energy. 41 (2016) I9691–I9701. doi:http://dx.doi.org/10.1016/j.ijhydene.2016.03.091.

[27] T. Tagaya, Y. Hatakeyama, S. Shiraishi, H. Tsukada, M.J. Mostazo-López, E. Morallón, D. Cazorla-Amorós, Nitrogen-Doped Seamless Activated Carbon Electrode with Excellent Durability for Electric Double Layer Capacitor, J. Electrochem. Soc. 167 (2020) 60523. doi:10.1149/1945-7111/ab8403.

[28] M.J. Mostazo-López, R. Ruiz-Rosas, S. Shiraishi, E. Morallón, D. Cazorla-Amorós, Nitrogen doped activated carbons prepared at mild conditions as electrodes for supercapacitors in organic electrolyte, J. Carbon Res. 6 (2020) 1–19. doi:10.3390/c6030056.

[29] D. Lozano-Castelló, M.A. Lillo-Ródenas, D. Cazorla-Amorós, A. Linares-Solano, Preparation of activated carbons from Spanish anthracite: I. Activation by KOH, Carbon. 39 (2001) 741–749. doi:10.1016/S0008-6223(00)00185-8.

[30] M.J. Mostazo-López, R. Ruiz-Rosas, E. Morallón, D. Cazorla-Amorós, Generation of nitrogen functionalities on activated carbons by amidation reactions and Hofmann rearrangement: Chemical and electrochemical characterization, Carbon. 91 (2015)

252–265. doi:10.1016/j.carbon.2015.04.089.

[31] D. Cazorla-Amorós, J. Alcañiz-Monge, M.A. De La Casa-Lillo, A. Linares-Solano, CO2 as an adsorptive to characterize carbon molecular sieves and activated carbons, Langmuir. 14 (1998) 4589–4596. http://www.scopus.com/inward/record.url?eid=2-s2.0-0032482837&partnerID=tZOtx3y1.

[32] J. Jagiello, J.P. Olivier, 2D-NLDFT adsorption models for carbon slit-shaped pores with surface energetical heterogeneity and geometrical corrugation, Carbon. 55 (2013) 70–80. doi:10.1016/j.carbon.2012.12.011.

[33] C. Schütter, C. Ramirez-Castro, M. Oljaca, S. Passerini, M. Winter, A. Balducci, Activated carbon, carbon blacks and graphene based nanoplatelets as active materials for electrochemical double layer capacitors: A comparative study, J. Electrochem. Soc. 162 (2015). doi:10.1149/2.0381501jes.

[34] D. Cazorla-Amorós, D. Lozano-Castelló, E. Morallón, M.J. Bleda-Martínez, A. Linares-Solano, S. Shiraishi, Measuring cycle efficiency and capacitance of chemically activated carbons in propylene carbonate, Carbon. 48 (2010) 1451–1456. doi:10.1016/j.carbon.2009.12.039.

[35] M. Hahn, A. Würsig, R. Gallay, P. Novák, R. Kötz, Gas evolution in activated carbon/propylene carbonate based double-layer capacitors, Electrochem. Commun. 7 (2005) 925–930. doi:10.1016/j.elecom.2005.06.015.

[36] P.W. Ruch, D. Cericola, A. Foelske-Schmitz, R. Kötz, A. Wokaun, Aging of electrochemical double layer capacitors with acetonitrile-based electrolyte at elevated voltages, Electrochim. Acta. 55 (2010) 4412–4420. doi:10.1016/j.electacta.2010.02.064.

[37] C.A. Leon y Leon, L.R. Radovic, Interfacial chemistry and electrochemistry of carbon surfaces, in: P.A. Thrower (Ed.), Chem. Phys. Carbon, Vol. 24, Marcel Dekker, Inc New York, 1994: pp. 213–310.

[38] A. Brandt, A. Balducci, Theoretical and practical energy limitations of organic and ionic liquid-based electrolytes for high voltage electrochemical double layer capacitors, J. Power Sources. 250 (2014) 343–351. doi:10.1016/J.JPOWSOUR.2013.10.147.

[39] G. Moreno-Fernández, C. Schütter, J.M. Rojo, S. Passerini, A. Balducci, T.A. Centeno, On the interaction of carbon electrodes and non conventional electrolytes in high-voltage electrochemical capacitors, J. Solid State Electrochem. 22 (2018) 717–725. doi:10.1007/s10008-017-3809-7.

[40] A.C. Forse, C. Merlet, J.M. Griffin, C.P. Grey, New perspectives on the charging mechanisms of supercapacitors, J. Am. Chem. Soc. 138 (2016) 5731–5744. doi:10.1021/jacs.6b02115.

[41] M. Salanne, B. Rotenberg, K. Naoi, K. Kaneko, P.-L. Taberna, C.P. Grey, B. Dunn, P. Simon, Efficient storage mechanisms for building better supercapacitors, Nat. Energy.

1 (2016) 16070. doi:10.1038/nenergy.2016.70.

[42] C. Largeot, C. Portet, J. Chmiola, P.-L. Taberna, Y. Gogotsi, P. Simon, Relation between the ion size and pore size for an electric double-layer capacitor, J. Am. Chem. Soc. 130 (2008) 2730–2731. doi:10.1016/j.carbon.2007.10.023.(15).

[43] D. Lozano-Castelló, D. Cazorla-Amorós, A. Linares-Solano, S. Shiraishi, H. Kurihara, A. Oya, Influence of pore structure and surface chemistry on electric double layer capacitance in non-aqueous electrolyte, Carbon. 41 (2003) 1765–1775. doi:10.1016/S0008-6223(03)00141-6.

[44] A. Balducci, R. Dugas, P.L. Taberna, P. Simon, D. Plée, M. Mastragostino, S. Passerini, High temperature carbon – carbon supercapacitor using ionic liquid as electrolyte, J. Power Sources. 165 (2007) 922–927. doi:10.1016/j.jpowsour.2006.12.048.

[45] D. Salinas-Torres, S. Shiraishi, E. Morallón, D. Cazorla-Amorós, Improvement of carbon materials performance by nitrogen functional groups in electrochemical capacitors in organic electrolyte at severe conditions, Carbon. 82 (2015) 205–213. doi:10.1016/j.carbon.2014.10.064.

[46] D. Hulicova-Jurcakova, M. Kodama, S. Shiraishi, H. Hatori, Z.H. Zhu, G.Q. Lu, Nitrogen-Enriched Nonporous Carbon Electrodes with Extraordinary Supercapacitance, Adv. Funct. Mater. 19 (2009) 1800–1809. doi:10.1002/adfm.200801100.

[47] H. Itoi, H. Nishihara, T. Kyotani, Effect of Heteroatoms in Ordered Microporous Carbons on Their Electrochemical Capacitance, Langmuir. 32 (2016) 11997–12004. doi:10.1021/acs.langmuir.6b02667.

[48] C. Peng, S. Zhang, X. Zhou, G.Z. Chen, Unequalisation of electrode capacitances for enhanced energy capacity in asymmetrical supercapacitors, Energy Environ. Sci. 3 (2010) 1499–1502. doi:10.1039/c0ee00228c.

[49] E. Redondo, W.-Y. Tsai, B. Daffos, P.-L. Taberna, P. Simon, E. Goikolea, R. Mysyk, Outstanding room-temperature capacitance of biomass-derived microporous carbons in ionic liquid electrolyte, Electrochem. Commun. 79 (2017) 5–8. doi:http://dx.doi.org/10.1093/deafed/enn036.

[50] Y. Zhu, M. Chen, Y. zhang, W. Zhao, C. Wang, A biomass-derived nitrogen-doped porous carbon for high-energy supercapacitor, Carbon. 140 (2018) 404–412. doi:S0008622318308170.

[51] M. Sevilla, N. Diez, G.A. Ferrero, A.B. Fuertes, Sustainable supercapacitor electrodes produced by the activation of biomass with sodium thiosulfate, Energy Storage Mater. 18 (2019) 356–365. doi:10.1016/j.ensm.2019.01.023.

[52] V.V. Strelko, V.S. Kuts, P.A. Thrower, On the mechanism of possible influence of heteroatoms of nitrogen, boron and phosphorus in a carbon matrix on the catalytic

activity of carbons in electron transfer reactions, Carbon. 38 (2000) 1499–1503. doi:10.1016/S0008-6223(00)00121-4.

[53] M.J. Mostazo-López, R. Ruiz-Rosas, A. Castro-Muñiz, H. Nishihara, T. Kyotani, E. Morallón, D. Cazorla-Amorós, Ultraporous nitrogen-doped zeolite-templated carbon for high power density aqueous-based supercapacitors, Carbon. 129 (2018) 510–519. doi:10.1016/j.carbon.2017.12.050.

Supplementary Data

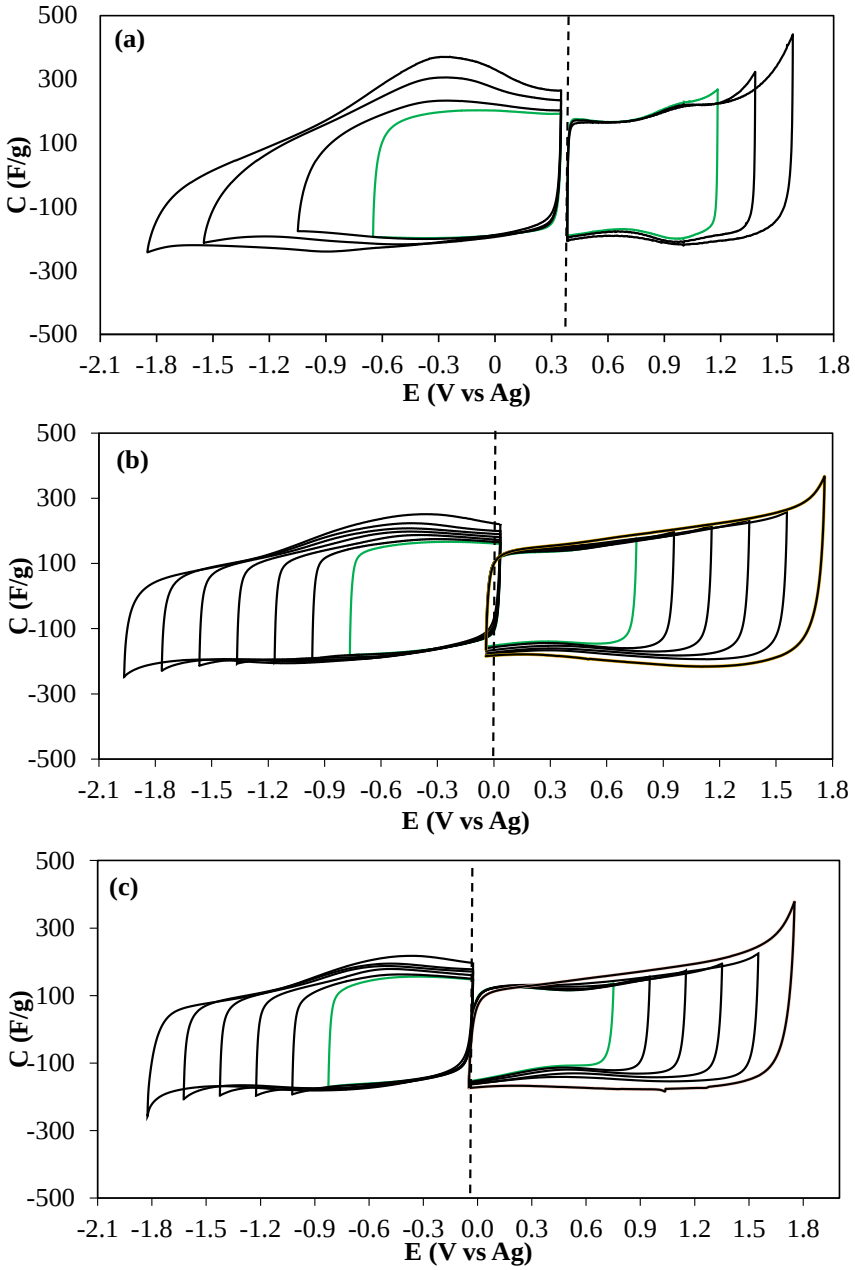

Figure S1. Cyclic voltammograms obtained for (a) KUA, (b) KUA-N and (c) KUA-$CONH_2$ electrodes under positive and negative polarization. 1M $Pyr_{14}BF_4$/PC. v = 1 mV/s.

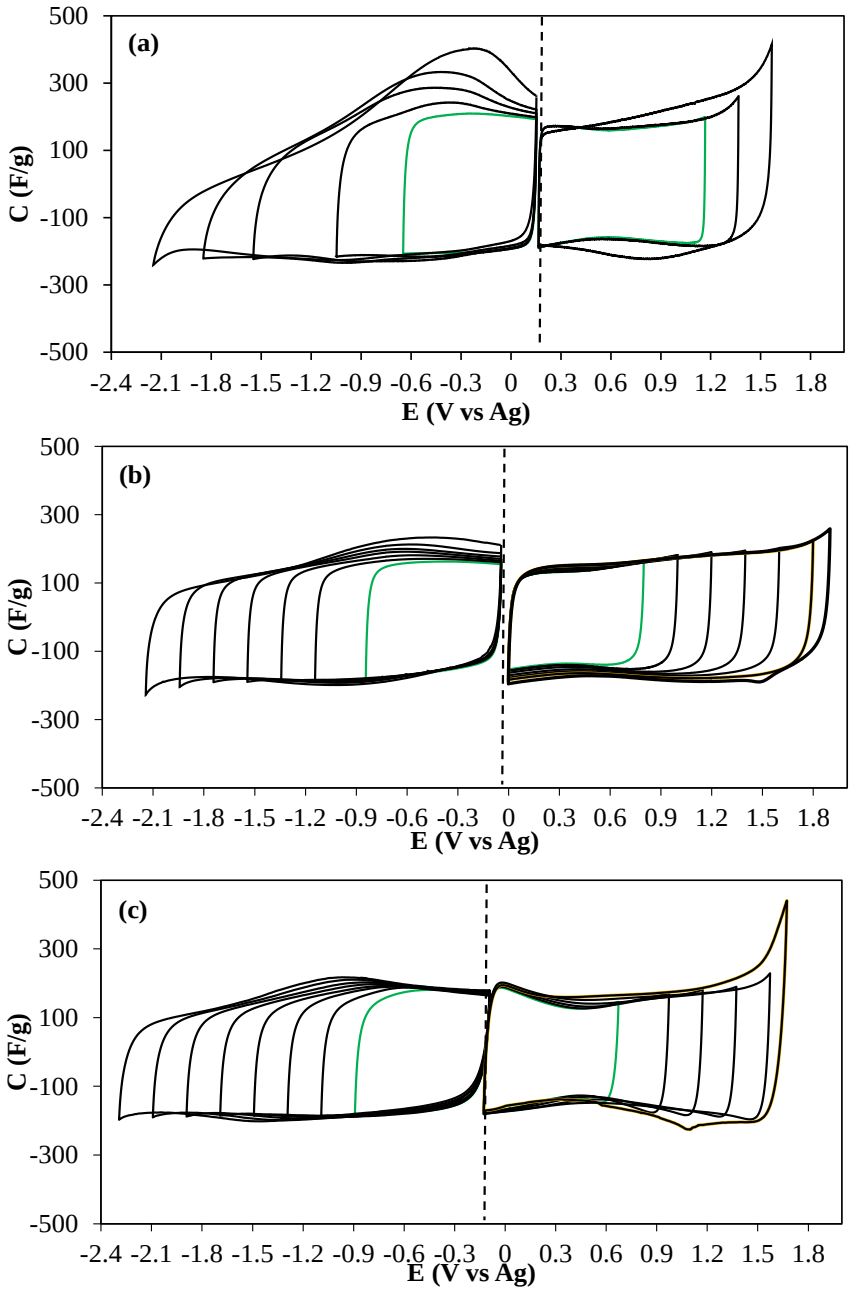

Figure S2. Cyclic voltammograms obtained for (a) KUA, (b) KUA-N and (c) KUA-$CONH_2$ electrodes under positive and negative polarization. 1M $Pyr_{14}TFSI$/PC. v = 1 mV/s.

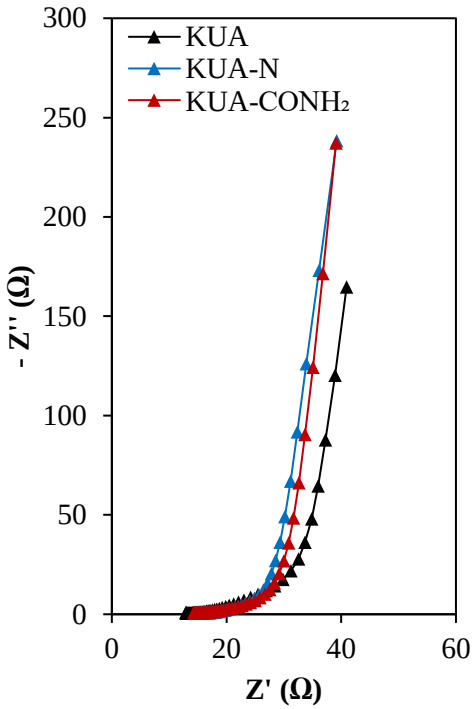

Figure S3. Electrochemical impedance spectra for KUA, KUA-N and KUA-CONH2 based supercapacitors. V = 0.05 V. 1M Pyr_{14}TFSI/PC.

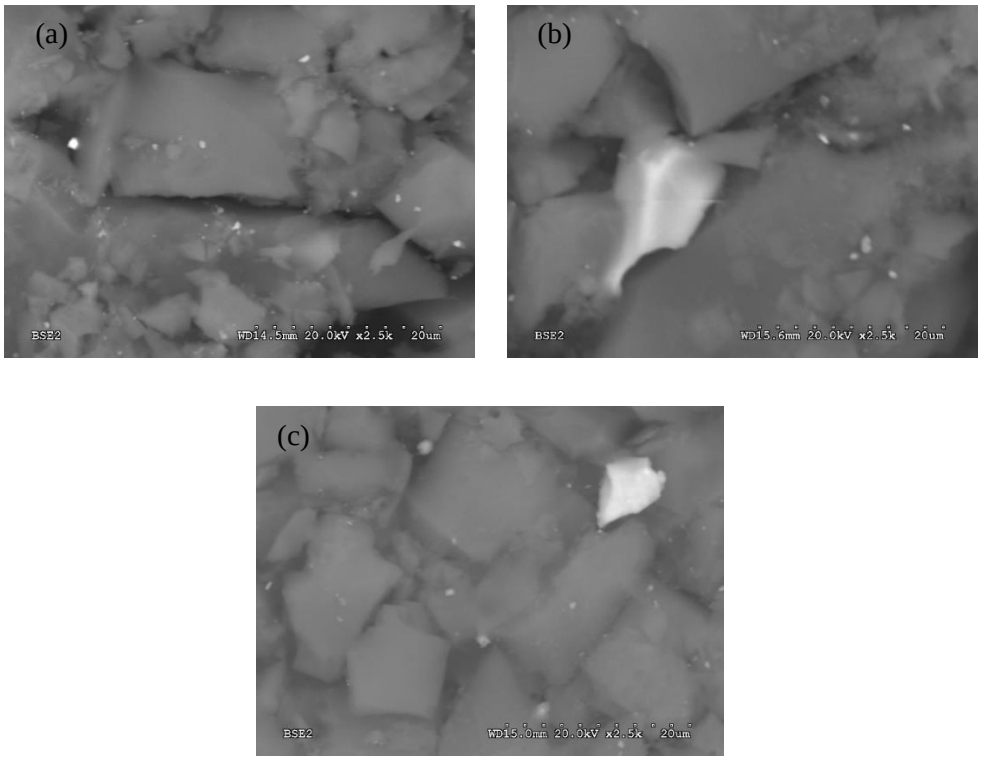

Figure S4. SEM images obtained for (a) KUA, (b) KUA-N and (c) KUA-$CONH_2$ fresh electrodes.

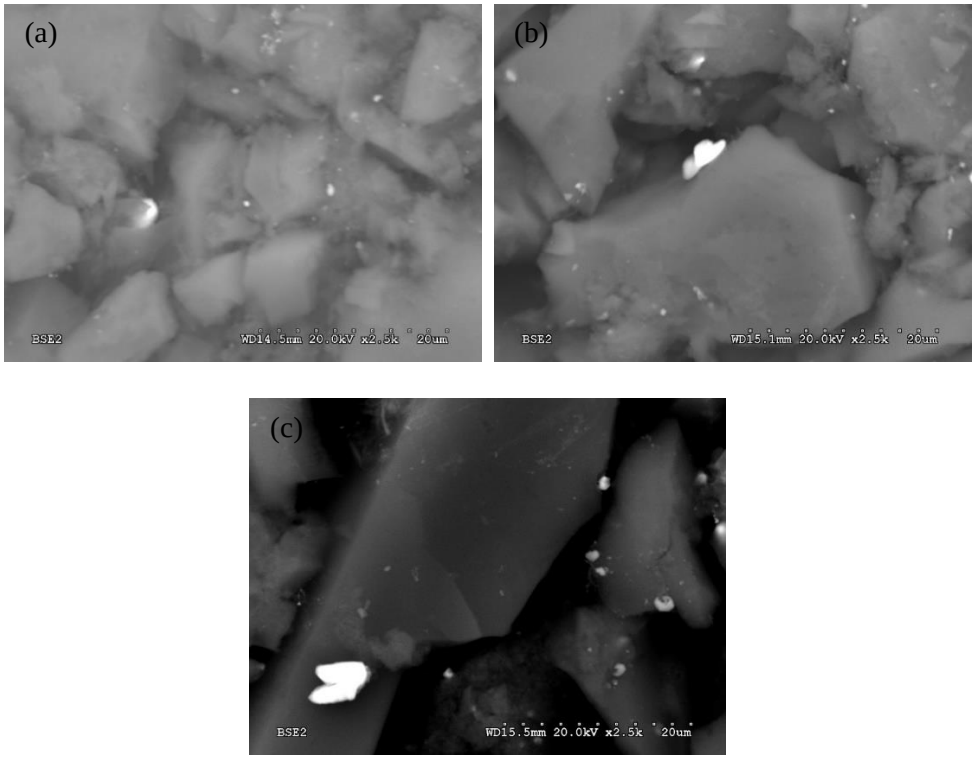

Figure S5. SEM images obtained for (a) KUA, (b) KUA-N and (c) KUA-$CONH_2$ positive electrodes after cycling.

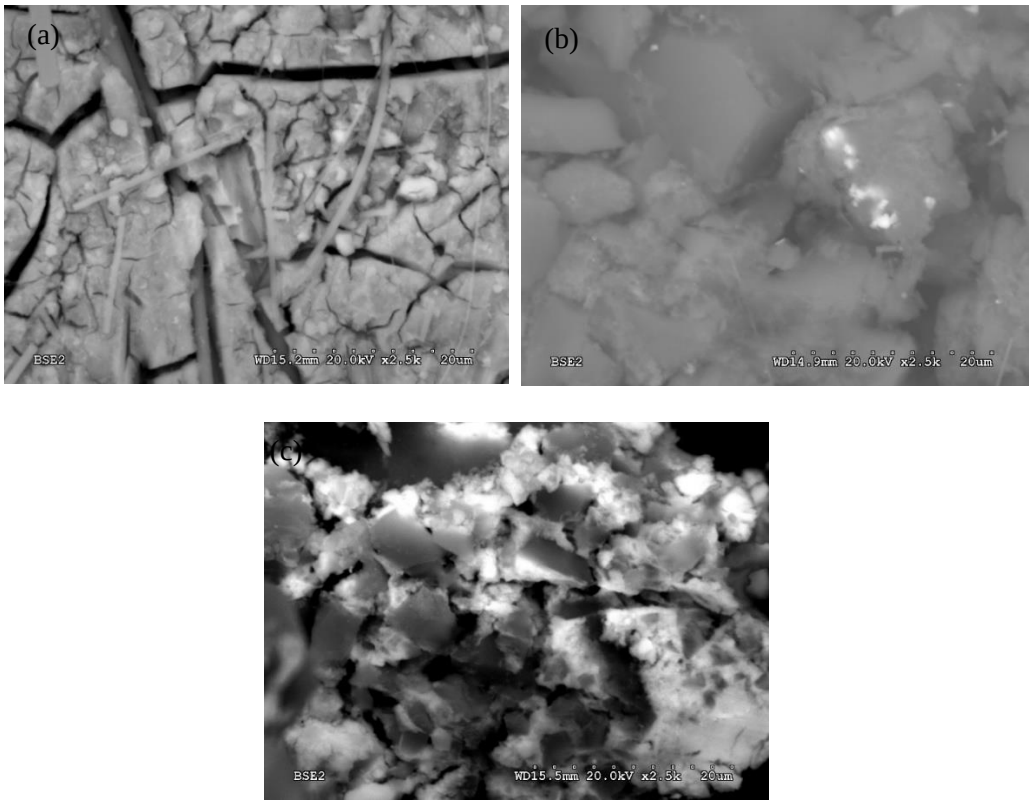

Figure S6. SEM images obtained for (a) KUA, (b) KUA-N and (c) KUA-$CONH_2$ negative electrodes after cycling.

Table S1. Surface composition obtained by SEM-EDX for the electrodes (before and after cycling).

Sample	C (at. %)	N (at. %)	O (at. %)	F (at. %)	Si (at. %)	Cr (at. %)	Fe (at. %)	S (at. %)	Other elements* (at. %)
KUA	93.88	-	4.46	1.60	-	-	-	0.07	-
KUA-N	87.64	5.78	5.10	1.13	-	-	-	-	-
KUA-$CONH_2$	82.19	9.03	7.20	1.45	-	0.05	-	-	0.07
KUA (+)	85.59	-	9.82	3.25	0.36	0.26	0.27	0.45	-
KUA-N (+)	81.86	6.15	6.61	4.31	0.09	0.16	0.13	0.69	-
KUA-$CONH_2$ (+)	81.93	7.02	9.17	1.12	0.11	0.27	0.09	0.09	0.20
KUA (-)	81.43	-	14.04	2.60	0.70	0.22	0.27	0.42	0.07
KUA-N (-)	88.52	-	7.88	2.53	-	0.28	1.85	0.35	-
KUA-$CONH_2$ (-)	69.87	-	23.44	2.44	0.07	0.48	2.78	0.38	0.56

***** Other elements (Mn, Ni, Cu, Al and Cl) were also detected in some samples.